Proceedings of FEDSM'03
2003 ASME_JSME Joint Fluids Engineering Conference
July 6-10, 2003, Honolulu, Hawaii USA

FEDSM2003-45635

ON NUMERICAL PREDICTION OF THE STABILITY OF HYPERSONIC BOUNDARY-LAYER FLOW OVER A ROW OF MICROCAVITIES

Vassilios Theofilis*
Dept. Motopropulsion y Termofluidodinámica,
E.T.S.I.A. Universidad Politécnica de Madrid,
Pza. Cardenal Cisneros 3, E-28040 Madrid, SPAIN

Michel O. Deville
Laboratoire d'ingénierie numérique
École Polytechnique Fédérale de Lausanne
CH-1015 Ecublens, Lausanne, SWITZERLAND

Peter W. Duck
Department of Mathematics
University of Manchester, Manchester M13 9PL, UK

Alexander Fedorov
Moscow Institute of Physics and Technology
141700 Moscow Region, RUSSIA

ABSTRACT

This paper is concerned with the structure of steady two–dimensional flow inside the viscous sublayer in hypersonic boundary–layer flow over a flat surface in which microscopic cavities ('microcavities') are embedded. Such a so–called Ultra Absorptive Coating (UAC) has been predicted theoretically [1] and demonstrated experimentally [2] to stabilize passively hypersonic boundary–layer flow.

In an effort to further quantify the physical mechanism leading to flow stabilization, this paper focuses on the nature of the basic flows developing in the configuration in question. Direct numerical simulations are performed, addressing firstly steady flow inside a singe microcavity, driven by a constant shear, and secondly a model of a UAC surface in which the two–dimensional boundary layer over a flat plate and a minimum nontrivial of two microcavities embedded in the wall are solved in a coupled manner. The influence of flow– and geometric parameters on the obtained solutions is illustrated. Based on the results obtained, the limitations of currently used theoretical methodologies for the description of flow instability are identified and suggestions for the improved prediction of the instability characteristics of UAC surfaces are discussed.

NOMENCLATURE

Latin symbols

d	microcavity diameter
D	microcavity depth
f	forcing frequency
Re	Reynolds number
s	spacing between successive microcavities
t	time
$(u,v)^T$	basic flow velocity vector
x,y	Cartesian coordinates

Greek symbols

ε	infinitesimal quantity
ν	kinematic viscosity
ψ	stream function

Subscripts

x, y	$\partial/\partial x, \partial/\partial y$

*Address all correspondence to this author.

INTRODUCTION

Interest in instability and control of a hypersonic boundary layer has been raised by the recent discovery of Fedorov and Malmuth [1] and Rasheed *et al.* [2], who have demonstrated theoretically and experimentally, respectively, that mode II instability, which prevails in hypersonic boundary–layer flow under a variety of environmental conditions, can be effectively controlled passively by coating the surface on which the instability develops by a porous material. A schematic representation of the Ultra–Absorptive Coating (UAC) surface employed is shown in Fig. 1. The key feature of this technology is the large disparity of scales between a typical mode II wavelength and the diameter d of each of the microscopic cavities on the coating. The porous material can thus be modeled by a row of cavities which are embedded at a characteristic distance s from each other inside the wall–coating; the cavities are of small size compared with the thickness of the boundary layer and are referred to as *microcavities*. In their immediate vicinity the external boundary–flow can be considered as driving flow inside each microcavity by a constant shear, as schematically depicted in Fig. 1. The optimal distribution of the microcavities on the coating surface is currently limited by the unknown nature of the interaction between the flowfields in the immediate vicinity of neighboring microcavities, which has provided motivation for the present work.

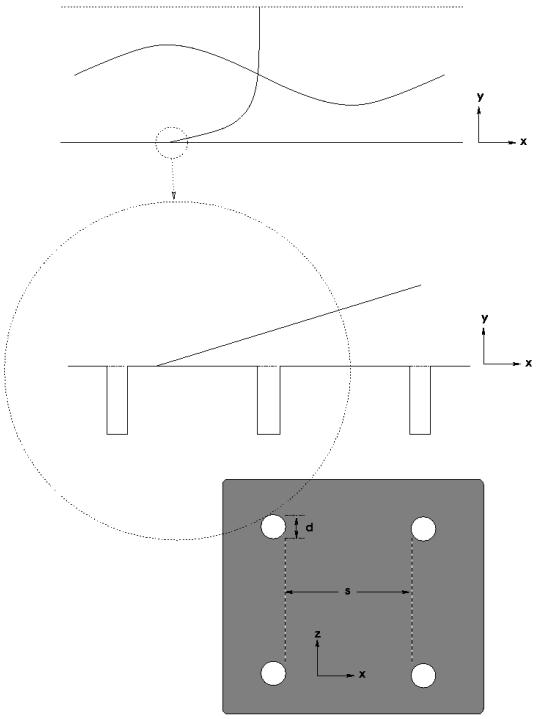

Figure 1. SCHEMATIC REPRESENTATION OF THE UAC SURFACE [3]

This paper and associated recent theoretical efforts intend to contribute to a better understanding of the flow inside porous coatings by providing detailed numerical predictions of the flowfield in the neighborhood of UAC surfaces, thus extending the original theoretical investigations of Fedorov and Malmuth [1] who have used an integral condition to model the effect of the microcavities on the hypersonic boundary layer. Two different approaches have been followed in the present work; the first considers independently the regimes of boundary–layer flow over the porous wall [4] and that inside an isolated microcavity [3] and the boundary condition at the open end of the microcavity is used to provide the link between the two flow regimes. In this approach, two aspects of the problem have been considered numerically, recovery of two–dimensional, essentially nonparallel basic states and three–dimensional BiGlobal instability analysis of such basic states [5]. Only basic flow results are discussed here and are contrasted with those of a second approach, which questions the conclusions put forward in all previous theoretical analyses by presenting, for the first time, results on the basic flow in the near–wall region of the UAC surface, obtained using spatial direct numerical simulation (DNS) based on a highly-accurate spectral–element approach.

The present analysis relies heavily on the slow nature of the flow in the immediate vicinity of the UAC surface. Indeed, previous work [1, 4, 5] has argued that, firstly, the flow inside the microcavity is expected to be of a viscous nature, driven by a constant shear at the open end of the microcavity and, secondly, that an incompressible model may be used for the description of the basic state in the immediate vicinity of the microcavities. Results were first obtained in a single microcavity, in which the outer (boundary–layer) flow was assumed to affect the inner (cavity) flow, but not vice-versa. The nature of two–dimensional basic flow inside a microcavity driven by a uniform shear-stress on one face was established by use of an accurate and efficient eigenvalue decomposition algorithm for DNS. The results obtained in this configuration were perturbed by small–amplitude harmonic perturbations superimposed at the lip of the microcavity. This extension is necessary in order to permit a more interactive regime, especially with respect to the perturbed flow. In particular a more realistic boundary condition recently suggested by [4] can be used to relate the wall–normal component of the disturbance velocity and disturbance pressure on the external face of the cavity. Finally, the basic flow results obtained using the previous two sets of approximations have been put in perspective by performing (unsteady) spectral–element DNS of flow over the entire model UAC surface, which encompasses both the near–wall viscous sublayer part of the hypersonic boundary layer flow and two microcavities embedded in the wall.

RESULTS

Single cavity, steady runs

The two–dimensional incompressible equations of motion have been solved using spectral collocation and a highly–efficient eigenvalue decomposition algorithm; details of the numerical approach are discussed by Theofilis [6]. The uniform tangential velocity at the cavity roof $y = D$ has been replaced by that of uniform wall shear stress. The issue of the singularity of the boundary conditions at the NE and NW corners of the cavity is thus absent in the present calculations and the time–accurate spectral collocation scheme utilized for the calculation of the basic flow demonstrates exponential convergence. Unlike the standard lid–driven cavity problem [7,8], in which the condition $\psi_y = 1$ is imposed at the N boundary and defines the effective flow Reynolds number, there is some ambiguity in the definition of a Reynolds number in the present case. Given that in the present approach the roof shear stress is constant (or $\psi_{yy} = 1$), the input Reynolds number may be regarded as either of

$$Re = u_y(y = D)d^2/\nu, \quad \text{or} \quad Re_{\text{int}} = \frac{1}{\nu}\int_{x=0}^{d} u(x, y = D)\, dx, \quad (1)$$

ν being the kinematic viscosity of the fluid. While ν is a fixed parameter in the basic flow calculation code, $u(x, y = D)$ is unknown *a priori* and is determined from the converged basic–flow field. Taking $d = D = 1$ basic flow results have been obtained using a rectangular grid comprising upwards of 96 collocation points per spatial direction. These have been compared against the classic lid–driven cavity flow [7], the Reynolds number in the latter case taken to be of $O(Re_{\text{int}})$ in the former; this comparison points to a general qualitative agreement between the two model flows, discussed in some detail in [3, 5].

Single cavity, unsteady runs

Next, the DNS algorithm has been modified to address unsteadiness at the microcavity lip, generated by instability in the external field which penetrates inside the microcavity, or unsteadiness due to resonance originating inside the microcavity which propagates in the boundary layer. This coupling is pivotal in order to combine the analytic/numeric approach of [4] in the external boundary layer flow with the present fully numerical approach required to describe flow inside the microcavity.

To this end, a $D = 2$ microcavity has been considered and a linear harmonic forcing has been imposed upon the flow at the N boundary. Representative results are shown at $Re = 100$, in the form of time–dependence of a flow quantity at a given position in the flowfield in Fig. 2; here u is monitored, although others exhibit qualitatively analogous behavior. In Fig. 2 it can be seen that, starting from rest, at $t < 20$ a steady state solution is approached. When non–zero amplitude forcing is applied at

Table 1. PARAMETERS FOR THE SINGLE–CAVITY UNSTEADY DNS

t	ε	f
< 20	0	0
$20 < t < 40$	10^{-4}	1
$40 < t < 60$	10^{-4}	0.5
> 60	0	0

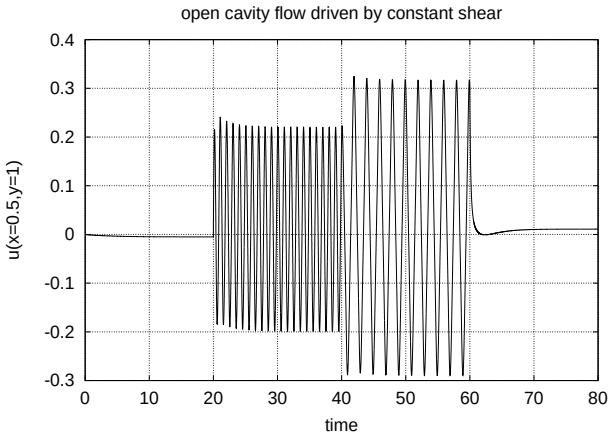

Figure 2. RESPONSE OF THE FLOW INSIDE A MICROCAVITY SET UP BY A SHEAR WHICH IS HARMONICALLY-DEPENDENT ON TIME DURING $t \in [20, 60]$. SHOWN IS $u(x = 0.5, y = 1; t)$.

the N boundary of the cavity, the flow responds linearly in a periodic manner. After rather short transients following the (Heaviside) changes of the forcing amplitude ε at $t = 20$ and of f at $t = 40$, the flow settles to two different harmonic motions with periods $T_{20-40} = 1/f = 1$ at $20 \le t < 40$ and $T_{40-60} = 1/f = 2$ at $40 \le t < 60$. A snapshot of the normal velocity component solution at $t = 40$ is shown in Fig. 3. At $t = 60$ the forcing is removed and, by the end of the simulation, the flow approaches the same steady–state reached at $t = 20^-$. Convergence of the results presented has been demonstrated and qualitatively analogous results obtained at parameter values different to those presented in table 1 point to the fact that imposition of harmonic motion at the open end of the cavity sets up a linear response of the flow inside the cavity in resonance with the imposed frequency, provided that the forcing amplitude is kept small. Another potentially significant result for subsequent modeling is the finding that the bulk of the fluid flow motion, both unforced and forced, is confined within a depth approximately equal to the length of the microcavity, as also shown in Fig. 3.

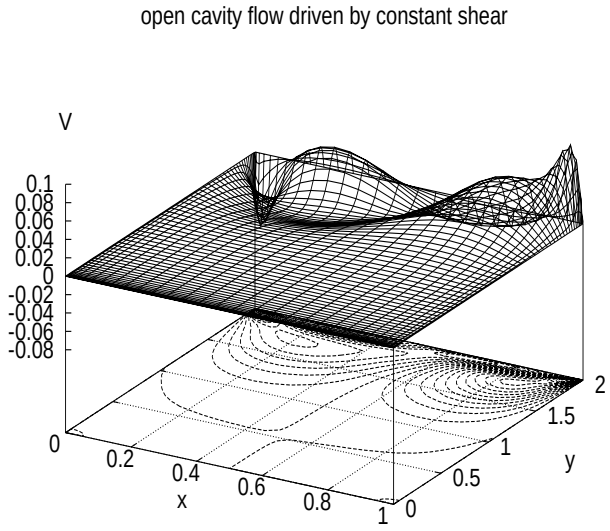

Figure 3. A SNAPSHOT, AT $t = 40$, OF THE NORMAL VELOCITY COMPONENT OF THE PERIODIC FLOW OF FIG. 2

Two microcavities, unsteady runs

The results of the previous sections are next compared with those obtained in a model UAC surface, encompassing the minimum nontrivial number of two microcavities embedded into the wall, as schematically depicted in Fig. 4. Consistent with the previous sections a two–dimensional approximation is made and a spectral–/mortar–element methodology [9] is used to discretize space. The equations of motion are solved in primitive variables and time–integration proceeds, using one of several alternative semi–implicit schemes available, until convergence to a steady state is obtained. The viscous boundary conditions at the walls are complemented by a constant shear imposed at the inflow W and farfield N boundaries, respectively, and natural boundary conditions of vanishing stresses, employed in the outflow E boundary. Simulations in the configuration shown in Fig. 4 require an order–of–magnitude larger computing effort compared with single–domain calculations and, hence, a limited amount of results monitoring variations of the essential flow parameters have been obtained. Nevertheless, results obtained suffice to highlight essential differences between the numerical solutions obtained in the previous two and the present section. Specifically, two questions have been posed and answered:

- First, how does the flowfield in the near–microcavity region compare with solutions obtained using the assumptions of earlier theoretical work by Fedorov and Malmuth [1]?

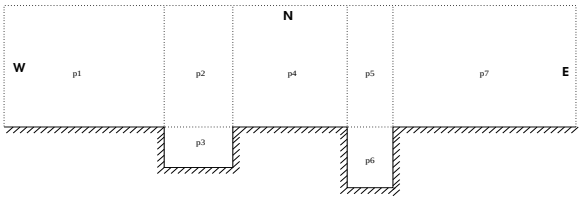

Figure 4. SKETCH OF THE GEOMETRY CONSIDERED

- Second, how do the geometric parameters s and D affect the flowfield of a microcavity (including the induced boundary–layer flow) and the interaction of this flowfield with neighboring microcavities?

Answers to these questions can provide guidance to theory through identification of the range of minimum spacing/depth of microcavities for which the integral conditions used by Fedorov and Malmuth [1] hold, and to experiment, through use of this information when manufacturing materials whose stability properties are reliably predicted by theory.

Taking $L = d = D = 1$, some numerical experimentation was necessary in order to determine the remaining geometric parameters, such that (a) the location of the inflow boundary does not interfere with the flowfield in the neighborhood of the upstream microcavity, on the one hand permitting the boundary layer to develop on the upstream wall of the configuration and on the other hand not placing excessive resolution requirements on account of a long upstream domain, (b) the location of the outflow boundary be placed well downstream of the downstream cavity, such that the outflow boundary conditions are physically plausible and, finally, (c) the location at which the domain is truncated in the $y-$spatial direction be such that activity taking place in the neighborhood of the microcavities is not affected by this (artificial) domain truncation.

Having satisfied these three requirements, the remaining physical parameters to be determined were the Reynolds number and the distance s between the microcavities. Related numerical parameters were the time–step Δt of the unsteady simulations and the number of subdomains in which each of the parent subdomains ($p_1 - p_7$ in Fig. 4) was to be subdivided, as well as the degree of polynomial approximation within each subdomain. The last two parameters determine the convergence properties of the algorithm and the accuracy of the solutions obtained and are (alongside Re) linked with Δt via the CFL condition.

Results have been obtained for $Re \in [10, 10^3]$ and $s \in [1, 4]$ while, in order to verify the conclusion put forward in the previous section regarding the significance of the microcavity depth parameter, simulations comparing the results of $D = 1$ and 2 have also been performed. In all calculations each of the 7 parent subdomains $p_1 - p_7$ was further subdivided into 4^2 subdomains, within each of which flow quantities were resolved using a 7^{th}

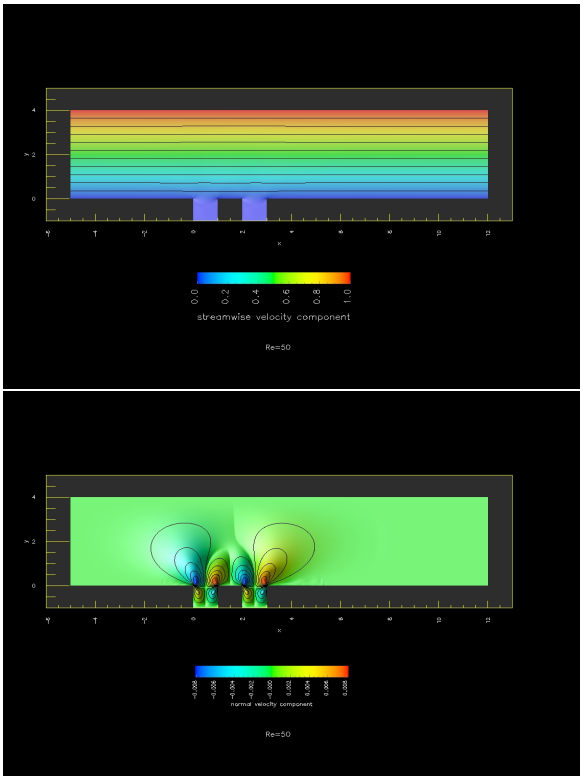

Figure 5. $Re = 50$ FLOW OVER TWO UNIT SQUARE MICROCAVITIES, SET APART BY $s = 1$. UPPER: STREAMWISE VELOCITY COMPONENT. LOWER: NORMAL VELOCITY COMPONENT

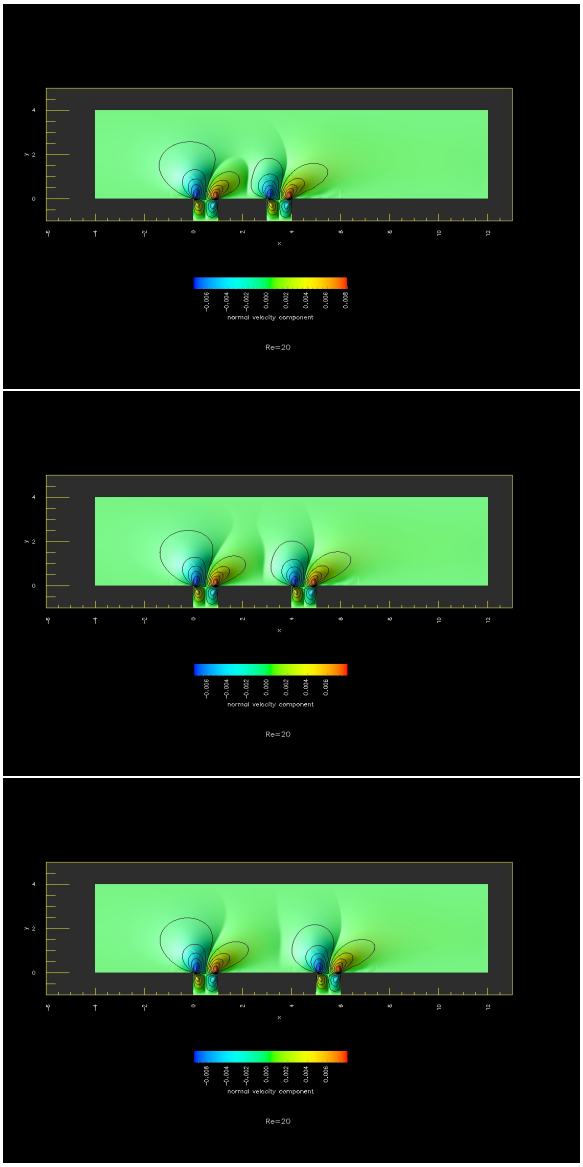

Figure 6. EFFECT OF SPACING $s \in [2,4]$ ON A TWO-UNIT-SQUARE-MICROCAVITY CONFIGURATION AT $Re = 20$.

degree polynomial. These values represent a compromise between accuracy and efficiency; resolving a parent subdomain using 2^2 subdomains and lower degree polynomials produces qualitatively correct results, while further increasing the number of subdomains ($6^2 \times 7 = 252$ being the next possibility, compared with the currently used $4^2 \times 7 = 112$ subdomains) was found to be unnecessarily expensive. In the parameter ranges explored the unsteady algorithm has yielded stationary solutions only; at convergence successive time–step results exhibit a relative time variation of less than 1×10^{-7}.

Of the results obtained most relevant for the problem at hand are low Reynolds number calculations [1, 4, 5]. The spatial distribution of the steady states for $u(x,y)$ and $v(x,y)$ at $Re = 50$ and $s = D = 1$ is presented in Fig. 5; the slow motion of flow inside the microcavity can be appreciated in this result. The normal (to the wall on which the boundary layer develops) velocity component reveals an interesting aspect of the flow. On the one hand, fluid in the microcavity is found to be in near–solid–body rotation, as expected by the smallness of the Reynolds number. On the other hand, compensation of this phenomenon takes place inside the boundary layer, where the presence of the microcavity appears to exert influence on the flow over a relatively large part of the domain outside the microcavity itself. The first result is in line with the assumption of the previous two sections and those of Fedorov and Malmuth [1] and Duck [4]. The second result is expected to have a strong influence on the stability characteristics of the boundary layer and can only be predicted numerically by simulations, such as these presented herein. Further inspection of the normal velocity component appears to suggest that $s = 1$ is a distance at which the fluid motion induced in the boundary layer by one microcavity interacts nonlinearly with that induced by its next neighbor. In other words, placement of microcavities

at distances $s \leq 1$ apart will prohibit application to a row of microcavities (in an integral manner) of analytical models derived on the basis of a single microcavity.

Next, the effect of s on the solutions obtained at constant Re and D is examined; representative results are presented in Fig. 6 at $Re = 20, D = 1$. It can be seen that $s \geq 4$ is necessary in order for the induced flowfields of two neighboring microcavities to become qualitatively similar. Unless three–dimensional instability modifies these basic flows, this result suggests that using such a spacing between microcavities can ensure that the model used to describe the induced flowfield of a single microcavity can be applied in an integral manner to describe the interaction between the boundary layer and a porous material. In the parameter ranges investigated, in which no unsteadiness occurs, the Reynolds–number effect, also examined, is substantially less pronounced than that of the spacing between microcavities. Finally, the conclusion of the previous sections that the bulk of the activity inside the microcavity takes place within a depth equal to the width of the microcavity has been confirmed in the framework of the present multiple–microcavity simulations; quantitative inspection of all solutions obtained in $y \in [-2, -1]$ revealed a rapid decay of all flow quantities with depth.

DISCUSSION

This paper is a first step in modeling the flow inside porous media coatings which are known to be useful in controlling hypersonic (in particular mode II) boundary–layer flow instabilities. Here direct numerical simulations have been performed to shed light upon the structure of the essentially incompressible viscous sublayer established inside the hypersonic boundary–layer on account of the presence of the microcavities. The first set of results obtained has assumed the outer flow to affect the inner (cavity) flow, but not vice-versa and established the nature of two–dimensional basic flow inside a microcavity driven by a uniform shear-stress. Some BiGlobal [6] instability results of this flow have also been obtained [5] and they strongly suggest the flow to be quite stable in likely practical regimes (Reynolds numbers), particularly when compared with the lid–driven cavity problem [8]. The second set of results obtained has permitted small–amplitude harmonic perturbations superimposed upon the solutions obtained in the first leg of the investigations. An isolated microcavity has been shown to respond to external forcing in a linear manner, periodic flow being set up inside the cavity at the imposed external frequency.

The basic flow results obtained using the previous two sets of approximations have been put in perspective by performing DNS of a model UAC surface. It has been shown that the parameter on which the flowfield most critically depends on is the spacing between microcavities; beyond a spacing $s \approx 4$ (which scales with other geometric parameters of the flow) it appears to be permissible to study microcavities in isolation from one–another (but interacting with the boundary layer) and calculate the effect of the induced flow motion on the boundary layer in an analytical (integral) manner. Other parameters, such as the depth of the cavities and the Reynolds number have been found to have a lesser impact on the flow, at least in the parameter range of interest where steady states prevail.

Future work aiming to aid optimization of microcavity scale and distribution should address the key issue left open in the current investigations, namely three–dimensionality. The most efficient means to accomplish this task is to study harmonic modifications of the present two–dimensional basic states in the third spatial direction, by employing BiGlobal instability analysis.

ACKNOWLEDGMENT

This material is based upon work supported by the European Office of Aerospace Research and Development, Air Force Office of Scientific Research, Air Force Research Laboratory, under Contracts No. F61775-01-WE046 and F61775-01-WE049 monitored by Mr. Wayne Donaldson and Dr. John D. Schmisseur.

REFERENCES

[1] Fedorov, A. V., and Malmuth, N. D., 2001. Stabilization of hypersonic boundary layer by porous coatings. Tech. Rep. 2001-0891, AIAA.

[2] Rasheed, A., Hornung, H. G., Fedorov, A., and Malmuth, N., 2001. Experiments on passive hypervelocity boundary-layer control using a porous surface. Tech. Rep. 2001-0274, AIAA.

[3] Theofilis, V., 2002. Numerical prediction of the hypersonic boundary-layer over a row of microcavities. Tech. Rep. F61775-01-WE049, EOARD.

[4] Duck, P. W., 2002. Theoretical prediction of the hypersonic boundary-layer over a row of microcavities. Tech. Rep. F61775-01-WE046, EOARD.

[5] Duck, P. W., and Theofilis, V., 2002. Flow and flow instability inside a microcavity. Tech. Rep. 02-2987, AIAA.

[6] Theofilis, V., 2003. "Advances in global instability of nonparalell and three–dimensional flows". *Prog. Aero. Sciences*, p. to appear.

[7] R. Schreiber, and H. B. Keller, 1983. "Driven cavity flows by efficient numerical techniques". *J. Comput. Physics*, **49**, pp. 310–433.

[8] Theofilis, V., 2000. Globally unstable basic flows in open cavities. Tech. Rep. 2000-1965, AIAA.

[9] Y. Dubois-Pèlerin, V. van Kemenade, and M. O. Deville, 1999. "An object–oriented toolbox for spectral element analysis". *J. Scient. Computing*, **14**, pp. 1–29.